Bulgarian Chemical Communications, Volume 49, Special Edition B (pp. 167 – 175) 2017

Copper, zinc and manganese spinel ferrites hosted in activated carbon from waste biomass as catalysts for hydrogen release from methanol

T. S. Tsoncheva[1]*, G. S. Issa[1], A. B. Mileva[1], R. N. Ivanova[1], M. D. Dimitrov[1], I. P. Spassova[2], D. G. Kovatcheva[2], D. G. Paneva[3], N. I. Velinov[3], B. G. Tsyntsarski[1], N. V. Petrov[1]

[1] *Institute of Organic Chemistry with Centre of Phytochemistry, Bulgarian Academy of Sciences, 1113 Sofia, Bulgaria*
[2] *Institute of General and Inorganic Chemistry, Bulgarian Academy of Sciences, 1113 Sofia, Bulgaria*
[3] *Institute of Catalysis, Bulgarian Academy of Sciences, 1113 Sofia, Bulgaria*

Received February 13, 2017; Revised March 06, 2017

Dedicated to Acad. Bogdan Kurtev on the occasion of his 100th birth anniversary

Activated carbon was prepared from peach stones and used as a host matrix of nanosized MFe_2O_4 (M = Cu, Zn, Mn) spinel ferrites. The obtained composites were characterized by Nitrogen physisorption, XRD, UV-Vis, FTIR, Moessbauer spectroscopy and TPR with hydrogen. Their catalytic behaviour was tested in methanol decomposition with a potential application as hydrogen carrier. Activated carbon based catalysts revealed higher catalytic activity but relatively low selectivity to syngas formation than their analogues hosted in mesoporous silica matrix. $ZnFe_2O_4$ is more appropriate active phase for the activated carbon support, while $CuFe_2O_4$ has higher activity on the silica matrix. The role of different supports on the state of catalytic active phase was discussed in detail.

Key words: activated carbon from waste biomass; spinel ferrites; methanol decomposition

INTRODUCTION

Recently, the energy crisis and the increased environmental problems forced the development of fuel cell technology. However, due to the limitation of the hydrogen storage technologies, the interest towards the development of integrated fuel processors, supplied with liquid fuel, which can release hydrogen in case of need, gains a considerable attention [1–3]. Methanol possesses more advantages, such as high H/C ratio, compatibility with the present gasoline infrastructures and possibility to be produced by well developed technologies from different sources, including waste and renewable ones [2, 4]. Among the various reforming processes, methanol decomposition is the simplest one producing syngas [2, 5 and refs therein]. In our previous study we demonstrated that spinel ferrites could be effective catalysts for methanol decomposition at relatively low temperatures [6–10]. Spinel ferrites can be described by the general formula AB_2O_4, where A and B stand for tetrahedral and octahedral cation sites in a close cubic packing of oxygen. In normal spinel ferrite structure, M^{2+} ions occupy tetrahedral (A) sites, while the majority of Fe^{3+} cations occupy the octahedral (B) ones, as it is the case of $ZnFe_2O_4$ [11]. In an inverse spinel structure, like $CuFe_2O_4$, half of Fe^{3+} ions occupy tetrahedral sites, while the M^{2+} ions together with the rest Fe^{3+} ions are situated in octahedral positions. In partially inverse spinel ferrites, like $MnFe_2O_4$, M^{2+} and Fe^{3+} occupy both tetrahedral and octahedral position in different proportion [3]. The ferrite structure offers close connectivity between the cations responsible for their interesting magnetic, electric, catalytic and photocatalytic properties, which are strongly influenced by the cationic distribution [12].

A reliable approach to produce cheaper and more active catalysts is their usage in nanoscale by deposition on suitable supports. Activated carbon (AC) can be used for this purpose due to its high surface area, special surface reactivity and porous structure [13]. The main drawback of the activated carbon based technologies, which make them costly and with restricted applicability, is the use of non-renewable and relatively expensive raw materials (such as coal and wood) for their production. Nowadays to attain better economic viability, the application of low-cost AC, derived from renewable materials, such as biomass, is preferred [14]. In our pioneer investigations we reported the role of AC texture and functional characteristics on the formation of highly dispersed and catalytic active copper, iron, manganese and cobalt nanoparticles [15, 16]. We also stressed on the reductive activity of AC support on the regulation of oxidative state of metal species both during the

* To whom all correspondence should be sent:
E-mail: *tsoncheva@orgchm.bas.bg*

preparation procedure and the catalytic process, which often leads to fast catalyst deactivation. The facile effect of binary systems, like $ZnFe_2O_4$ spinel ferrite, on the stabilization of highly active metal species was demonstrated in [17]. This study is focused on the understanding the role of metal ion in supported on activated carbon MFe_2O_4 spinel ferrites on their catalysts behaviour in methanol decomposition. For the purpose, AC derived from waste biomass (peach stones), was compared with mesoporous silica type KIT-6 as a host matrix of $CuFe_2O_4$, $MnFe_2O_4$ and $ZnFe_2O_4$ spinel ferrites.

EXPERIMENTAL

The activated carbon, denoted as ACP, was obtained by carbonization of peach stones in nitrogen atmosphere at 873 K and subsequent activation of the obtained product in flow of water vapour at 1123 K. The carbons were modified by incipient wetness impregnation with methanol solutions of $Fe(NO_3)_3.9H_2O$ and $Zn(NO_3)_2.6H_2O$, $Mn(NO_3)_2.4H_2O$ or $Cu(NO_3)_2.3H_2O$ (total metal content - 8 wt%; Fe/M = 2 (M = Zn, Mn or Cu)). The precursor decomposition was carried out in nitrogen flow at 773 K. For comparison similar modifications of mesoporous silica type KIT-6 [19] were obtained. The samples are denoted as CuFe/S, MnFe/S and ZnFe/S, where S stands for ACP or KIT-6 support.

The texture characteristics were determined by low-temperature nitrogen adsorption in a Quantachrome Instruments NOVA 1200e (USA) apparatus. Powder X-ray diffraction patterns were collected on Bruker D8 Advance diffractometer with Cu Kα radiation and LynxEye detector. The UV-Vis spectra were recorded on the powder samples using a Jasco V-650 apparatus. The IR spectra (KBr pellets) were recorded on a Bruker Vector 22 FTIR spectrometer. The Mossbauer spectra were obtained in air at room temperature with a Wissel (Wissenschaftliche Elektronik GmbH, Germany) electromechanical spectrometer using $^{57}Co/Rh$ source and α-Fe standard. The TPR/TG analyses were performed on a Setaram TG92 instrument in a flow of 50 vol% H_2 in Ar (100 cm^3 min^{-1}) and heating rate of 5 K min^{-1}.

Methanol conversion was carried out in a fixed bed flow reactor (0.055 g of catalyst), argon being used as a carrier gas (50 $cm^3.min^{-1}$). The methanol partial pressure was 1.57 kPa. The catalysts were tested under conditions of a temperature-programmed regime within the range of 350–770 K with heating rate of 1 $K.min^{-1}$. On-line gas chromatographic analyses were performed on HP apparatus equipped with flame ionization and thermo-conductivity detectors, on a PLOT Q column, using an absolute calibration method and a carbon based material balance.

RESULTS AND DISCUSSION

Texture and structure characterization

Nitrogen physisorption isotherms of parent and ferrite modified ACP are of type I-IV according to the IUPAC classification which is typical of materials with well developed micro-mesoporous texture (not presented). The calculated parameters (Table 1) reveal that all ACP based materials are characterized with high surface area (960–1260 $m^2.g^{-1}$) and pore volume of 0.4–0.6 $cm^3.g^{-1}$, mainly determined by the presence of micropores (V_{mes}/V_{mic} is about 0.3). The significant decrease in the BET surface area and pore volume of ACP after the modification evidences pore blocking due to metal particles deposition. The slight decrease in the V_{mes}/V_{mic} for CuFe/ACP and ZnFe/ACP as compared to pure ACP (Table 1) indicates a preferable location of metal species into the mesopores, while blocking of micropores in higher extent is considered for MnFe/ACP.

Table 1. Nitrogen physisorption data: S_{BET} (specific surface area), S_{mi} (specific surface area of micropores), V_t - total pore volume, V_{mi} - micropore volume, D_{av} - average pore diameter).

Sample	S_{BET}, m^2/g	S_{mi}, m^2/g	V_t, cm^3/g	V_{mi} cm^3/g	D_{av} nm	ΔS_{BET}, %	ΔV_{tot}, %	V_{mes}/V_{mic}
ACP	1258	1116	0.61	0.44	1.9			0.35
CuFe/ACP	994	885	0.49	0.37	1.9	21	20	0.32
MnFe/ACP	1004	893	0.49	0.35	1.9	20	20	0.40
ZnFe/ACP	965	866	0.46	0.35	1.9	23	24	0.31
KIT-6	872	278	1.23	0.14	8.1			7.78
CuFe/KIT-6	744	197	1.07	0.10	5.8	15	13	9.70
ZnFe/KIT6	561	108	0.80	0.05	5.7	36	35	15.00
MnFe/KIT-6	800	106	1.20	0.05	6.0	8	2	23.00

For comparison, the nitrogen physisorption isotherms of KIT-6 silica are of IV type with well pronounced step in the 0.6–0.8 partial pressure range and type I hysteresis loop (not shown), which reveals presence of cylindrical and almost uniform mesopores (Table 1). The changes in the textural parameters after KIT-6 modification are indication for some differences in the location of metal species within the silica porous structure. Almost random blocking of micro and mesopores could be assumed for CuFe/KIT-6, while preferable location into the micropores seems to be realized for ZnFe/KIT-6, and even in higher extent for MnFe/KIT-6 (Table 1).

The XRD patterns of parent ACP and its modifications (Fig. 1a) contains well defined reflections at about 25^o and 45 ^{o} 2θ which according to *Liou and Wu* [20] are due to the turbostratic structure in AC. The preservation of the reflections after the modification reveals absence of significant structural collapse of the support, which is in agreement with the nitrogen physisorption data (Table 1). All additional reflections at 30.1^o, 35.3^o, 42.6^o, 52.9^o, 56.7^o and 62.7^o in the pattern of ZnFe/ACP could be indexed to (220), (311), (400), (422), (511) and (440) planes of cubic $ZnFe_2O_4$ ferrite (pdf 089-1010) with average crystallite size of about 7 nm. The XRD pattern of parent KIT-6 (Fig.1b, inset) represents two well-distinguished reflections in the small-angle region, which could be assigned to the (211) and (220) planes of 3-D cubic structure of high quality material. The preservation of these main reflections after the modification procedures (not presented) reveals absence of structural collapse with the silica support. The XRD pattern of ZnFe/KIT-6 represents reflections of α-Fe_2O_3 and $ZnFe_2O_4$ phases with average crystallite size of 11–13 nm (Fig. 1b). Taking into account the nitrogen physisorption data (Table 1), one could be assumed that the blocking of micropores of silica support during the active phase deposition renders difficult the formation of ferrite phase and leads to segregation of relatively large hematite and ferrite particles on the external surface or nearby the pore openings. The broad reflections at about 34.6^o, 35.9^o, 37.1^o, 41.6^o, 43.6^o, 58.0^o, 62.0^o, 63.8^o and 74.7^o 2θ in the pattern of CuFe/ACP (Fig. 1a) could be indexed as (103), (211), (202), (004), (220), (321), (224), (400) and (413) diffractions of cubic $CuFe_2O_4$ (pdf 077-0427) with average crystallite size of 8 nm. An addition, impurity peaks of metallic Cu (pdf 085-1326) with average crystallite size of 2 nm is also distinguished, probably due to the reduction activity of carbon support during the preparation procedure. On contrary, the absence of any reflections in CuFe/KIT-6 pattern (Fig. 1b) reveals higher dispersion of loaded metal oxide phase in the silica matrix, probably due to its stabilization into the support mesopores (Table 1). The broad diffraction reflections in the pattern of MnFe/ACP correspond to face centered cubic $MnFe_2O_4$ (pdf 074-2403) with average crystallite size of 4 nm. It seems that the blocking of active phase into the micropores of silica support (Table1, Fig. 1b) provokes the formation of highly dispersed amorphous phase in MnFe/KIT-6.

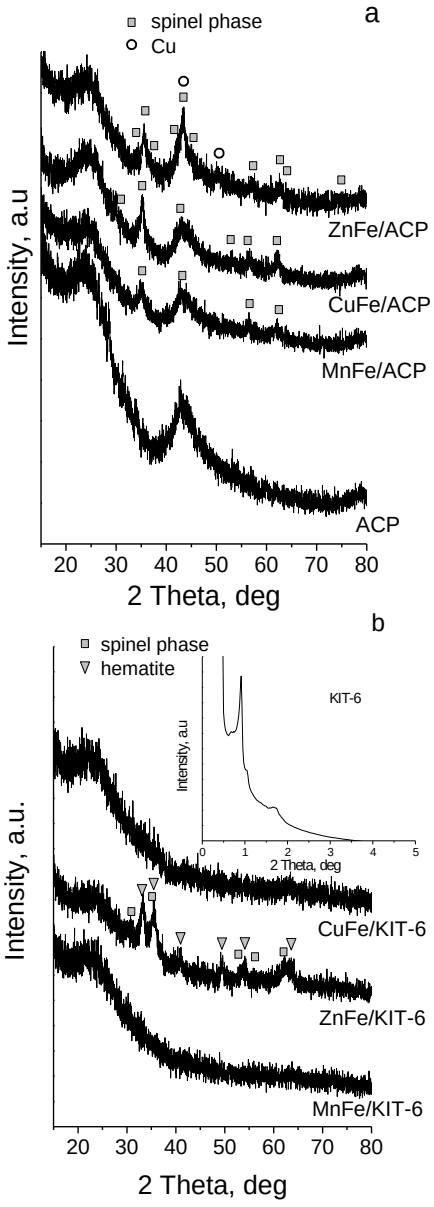

Fig. 1. XRD patterns of ACP (a) and KIT-6 (b) based samples before the catalytic test. Inset: low angle XRD pattern of KIT-6.

Spectroscopic measurements

FTIR spectra (Fig. 2) and Boehm method [17] are used for the characterization of AC surface functionality. The bands at *c.a.* 1360 cm^{-1} and 3000–2800 cm^{-1} could be assigned to asymmetric and symmetric –C–H stretching vibrations in aliphatic groups, while the strong band at around 1552 cm^{-1} is assigned to the vibrations in –C–C– aromatic bonds and C–O–O– structures [14].

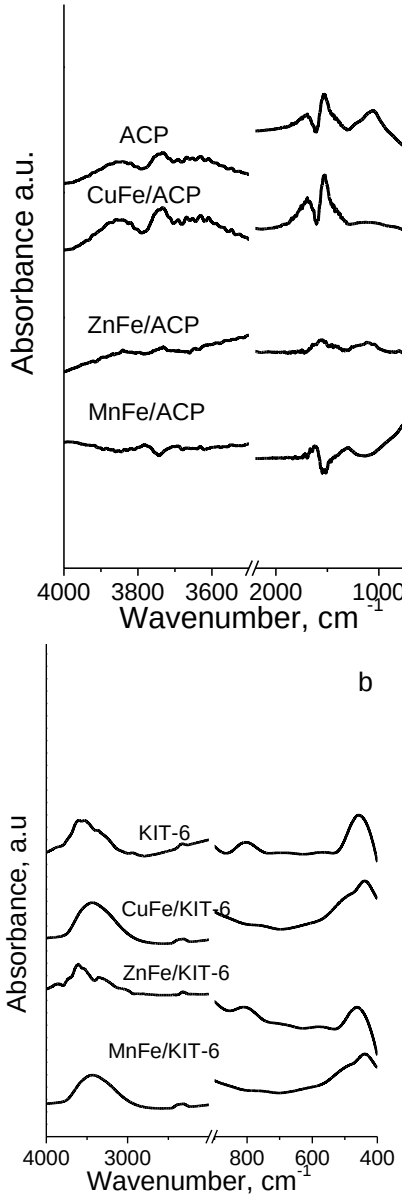

Fig. 2. FTIR spectra of ACP (a) and KIT-6 (b) ferrite modifications.

The band at *c.a.* 1044 cm^{-1} represents C–O stretching vibrations and the existence of a shoulder to the main peak is usually assigned to the positional differences among these functional groups. The observed decrease in the intensity of the absorption band at around 1550 cm^{-1} for CuFe/ACP and MnFe/ACP and at 1044 cm^{-1} for ZnFe/ACP could be due to the interaction of metal oxide species with π-electron structure and oxygen groups of carbon structure, respectively [21]. The band at 800–600 cm^{-1} can be attributed to C-C bending vibrations in aromatic and non-aromatic structures. The broad absorbance in the region 3644–3026 cm^{-1} is associated to residual water or –O–H stretching vibration mode of hydrogen bonded hydroxyl groups [14, 22]. The additional study by Boehm method reveals predominant presence of surface basic groups (1.04 mmol/g) as well as carbonyl (1.07 mmol/g) and hydroxyl (0.04 mmol/g) acidic ones. The appearance of two well pronounced bands at *c.a.* 600–500 cm^{-1} and 400–430 cm^{-1} in the FTIR spectra of CuFe/ACP and ZnFe/ACP (Fig. 2a) could be due to M-O stretching vibrations of metal ions in tetrahedral and octahedral positions in ferrite phase, respectively [22]. In case of MnFe/ACP, the presence of only one and broad band at *c.a.* 566 cm^{-1} slightly doubt the formation of ferrite phase and we'll return to this point with the Moessbauer spectroscopic study. For comparison, well pronounced bands, typical of ferrite phase, could be distinguished in the FTIR spectra of CuFe/KIT-6 and MnFe/KIT-6 (Fig. 2b). In consistence with the XRD data, the increased absorption at *c.a.* 566 cm^{-1} in the spectrum of ZnFe/KIT-6 could be ascribed to the co-existing of hematite and spinel phases [23]. The UV-Vis spectra of CuFe/KIT-6, ZnFe/KIT-6 and MnFe/KIT-6 represent absorption edges at 386, 518 and 391 nm, respectively which could be assigned to the presence of the corresponding ferrite particles. The significant deviation of the values for ZnFe/KIT-6 from the reported in the literature ones [24] could be assigned to the presence of impurities of Fe_2O_3, in consistence with the XRD and FTIR data (see above). Unfortunately the UV-Vis spectra of ACP based materials are not sufficiently representative. In order to obtain more information for the state of loaded ferrite phase in the parent materials and the changes with it during the catalytic test, room temperature Moessbauer spectra are collected and presented in Figs. 3a and 3b, respectively. The characteristic parameters: isomer shift (IS), quadruple splitting (QS), effective internal magnetic field (H_{eff}), the line width (FWHM) and the relative weight of each component (G), are presented in Table 2. The Moessbauer spectrum of parent CuFe/ACP (Fig. 3a. Table 2) represents superposition of doublet (Db)

and 3 sextets (Sx). The parameters of Sx1 and Sx2 correspond to tetrahedral and octahedral coordination of iron ions in magnetite structure, respectively. However, the presence of quadruple splitting, especially for octahedral coordinated iron (Sx2), shows that the magnetite is copper substituted. The third sextet component (Sx3) with low hyperfine field and broad line width might be attributed to additive effects of smaller magnetite particles, Fe^{3+} ions at the interface of non-structured $CuFe_2O_4$ and/or Fe^{3+} ions surrounded by more vacancies (and/or Cu^{2+} ions) [25]. The Db part of the spectrum indicates presence of finely dispersed (bellow 10–12 nm) Fe^{3+} containing nanoparticles with superparamagnetic (SPM) behavior. Obviously the carbon support promotes segregation of reduced phases (Cu^0 and $Cu_xFe_{3-x}O_4$) and restricts the formation of stoichiometric copper ferrite phase and (Fig. 3a) this is also confirmed by the XRD analyses (Fig. 1b). After the catalytic test (Fig. 3b, Table 2), new sextet component attributable to Fe_3C appears. On the base of relative weight of each component, phase transformations with the highly defective $Cu_xFe_{3-x}O_4$ particles under the influence of the reductive reaction medium could be assumed. For comparison, the Moessbauer spectrum of CuFe/KIT-6 represents only doublet. This tendency of stabilization of more finely dispersed phase into the micro/mesopores of silica support is confirmed with the XRD and nitrogen physisorption measurements. Note that no changes with the active phase could be mentioned after the catalytic test (Fig. 3b, Table 2). The spectrum of parent MnFe/ACP is well fitted with two sextets (Fig. 3a, Table 2). The broadening of both sextets could be explained with presence of particles with different size [25]. Formation of $MnFe_2O_4$ phase is also detected by XRD (Fig. 1a). The relatively high Db part in the Moessbauer spectrum of MnFe/ACP (about 78%) reveals presence of finely dispersed (below 10-12 nm) Fe^{3+} containing species. This is not surprised, taking account that these species are blocked predominantly into the micropores of ACP support (Table 1). This tendency is more pronounced for the MnFe/KIT sample, where the Moessbauer spectrum consists only of Db component. After the catalytic test (Fig. 3b, Table 2), the ferrite phase in parent MnFe/ACP, corresponding to the Sx component in the spectrum, is almost fully decomposed to magnetite. Just the opposite, no changes with the active phase could be assumed for MnFe/KIT-6. The spectrum of parent ZnFe/ACP (Fig. 3a, Table 2) represents a quadruple doublet with hyperfine parameters characteristic for $Zn_xFe_{3-x}O_4$ ferrite with relatively high Zn content ($x > 0.8$) [26]. The preservation of the spectrum after the catalytic test (Fig. 3b, Table 2) indicates stability of the ferrite phase under the reaction medium. For comparison, the Moessbauer spectrum of ZnFe/KIT-6 (Fig. 3a, Table 2) is superposition of 3 sextets. The parameters of Sx1 with relative weight of 15% correspond to Fe_2O_3 [26], in consistent with XRD data. The other two

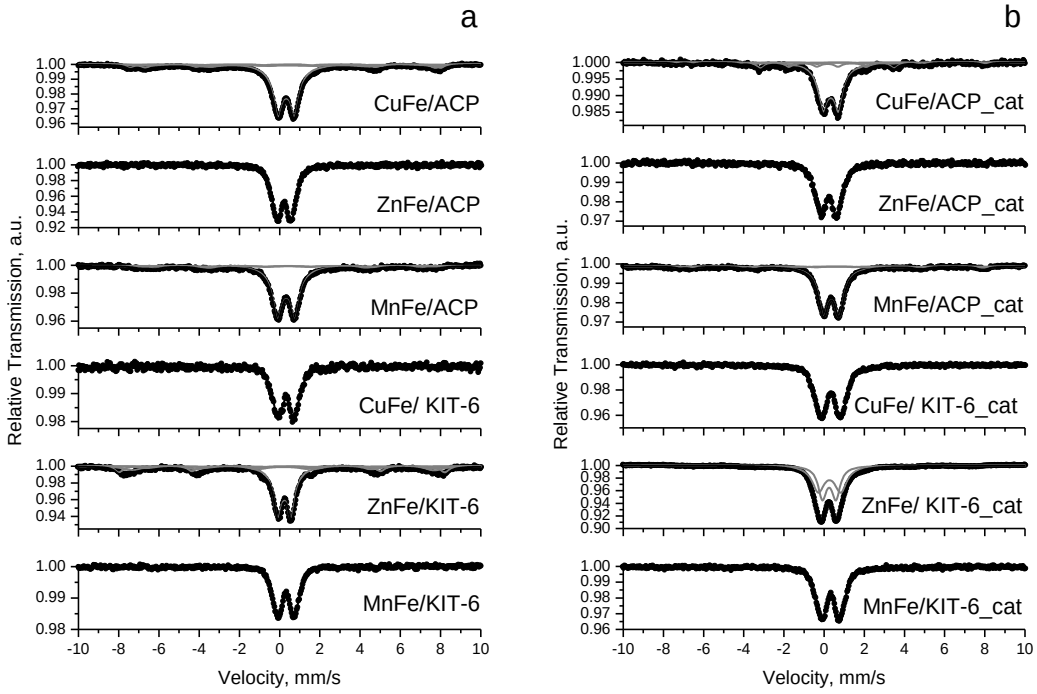

Fig. 3. Moessbauer spectra of all modifications before (a) and after (b) the catalytic test.

Table 2. Moessbauer parameters of ACP and KIT-6 modifications before and after (cat) the catalytic test.

Sample	Components	IS, mm/s	QS, mm/s	H_{eff}, T	FWHM, mm/s	G, %
CuFe/ACP	Sx1-Fe^{3+}_{tetra}, $Cu_xFe_{3-x}O_4$	0.30	-0.03	48.0	0.53	8
	Sx2-$Fe^{2.5+}_{octa}$, $Cu_xFe_{3-x}O_4$	0.58	-0.10	44.8	0.58	9
	Sx3-$Cu_xFe_{3-x}O_4$	0.40	0.06	40.2	1.80	18
	Db- SPM	0.33	0.81	-	0.62	65
ZnFe/ACP	Db - Fe^{3+}_{octa} , $Zn_xFe_{3-x}O_4$	0.35	0.74	-	0.58	100
MnFe/ACP	Sx1-Fe^{3+}_{tetra}, $MnFe_2O_4$	0.44	0.00	45.9	0.90	9
	Sx2-Fe^{3+}_{octa}, $MnFe_2O_4$	0.40	0.00	41.0	0.90	13
	Db-SPM	0.32	0.86	-	0.62	78
CuFe/ KIT-6	Db-SPM	0.32	0.82	-	0.60	100
ZnFe/KIT-6	Sx1 - Fe^{3+}_{octa} - α-Fe_2O_3	0.33	-0.11	50.4	0.50	15
	Sx2 - Fe^{3+}_{tetra} - $Zn_xFe_{3-x}O_4$	0.30	0.00	46.6	1.00	21
	Sx3 - $Fe^{2,5+}_{octa}$ - $Zn_xFe_{3-x}O_4$	0.64	0.00	43.5	1.20	10
	Db - $Zn_yFe_{3-x}O_4$	0.34	0.67	-	0.51	54
MnFe/KIT-6	Db-SPM	0.32	0.84	-	0.55	100
CuFe/ACP_cat	Sx1-Fe^{3+}_{tetra}, $Fe_{3-x}O_4$	0.28	0.00	47.5	0.45	4
	Sx2-$Fe^{2.5+}_{octa}$, $Fe_{3-x}O_4$	0.80	0.00	45.4	0.45	5
	Sx3-Fe_3C	0.16	0.00	20.7	0.47	17
	Db- SPM	0.34	0.76	-	0.65	74
CuFe/ KIT-6_cat	Db-SPM	0.34	1.00	-	0.68	100
ZnFe/ACP_cat	Db - Fe^{3+}_{octa}, $Zn_xFe_{3-x}O_4$	0.34	0.80	-	0.64	100
ZnFe/ KIT-6_cat	Db1 - Fe^{3+}_{octa}, $Zn_xFe_{3-x}O_4$	0.36	0.68	-	0.50	46
	Db2 - SPM	0.37	1.12	-	0.73	54
MnFe/ACP_cat	Sx1-Fe^{3+}_{tetra}, $Fe_{3-x}O_4$	0.28	0.00	46.4	0.50	5
	Sx2-$Fe^{2.5+}_{octa}$, $Fe_{3-x}O_4$	0.74	-0.03	45.2	0.54	8
	Db- SPM	0.36	0.79	-	0.61	87
MnFe/KIT-6_cat	Db-SPM	0.33	0.92	-	0.62	100

sextets with relatively high FWHM and G = 31 % could be assigned to non-stoichiometric $Zn_xFe_{3-x}O_4$ ferrite with relatively low Zn content [26]. The parameters of Db part of the spectrum are typical of ferrite phase with high degree of Zn substitution. The changes in the spectrum after the catalytic test (Fig. 3b, Table 2) reveal reduction transformation of the active phase under the reaction medium with the formation of finely dispersed iron oxides and/or carbides (Table 2).

TPR study

The TPR method is a feasible, but sometimes difficult for the interpretation, approach to characterize the oxidative state of metallic ions and the defectiveness of metal oxide crystal lattice. In Fig. 4 are presented TPR-TG and TPR-DTG profiles of all ACP and KIT-6 modifications. The reduction decomposition of CuFe/KIT-6 to Cu^0 and magnetite starts at 450 K followed by fast magnetite reduction to metallic iron [27]. The appearance of only one reduction effect with a maximum at 593 K confirms the facilitated reduction of magnetite due to the spillover of activated on copper species hydrogen [28]. The reduction profile of CuFe/ACP exhibits two well distinguished peaks indicating complex composition of the loaded metal phase. This result well corresponds to the XRD and Moessbauer data (Fig. 1, Table 2) for the co-existence of Cu and partially reduced $Cu_xFe_{3-x}O_4$ and confirms the obstructive role of AC support for the stoichiometric copper ferrite formation. The reduction decomposition of $MnFe_2O_4$ to MnO and magnetite and its further reduction to metallic iron is about 130 K shifted to higher temperatures as compared to CuFe/KIT-6. The absence of well distinguished additional low temperature effects and the symmetry of the main TPR-DTG effect clearly indicate the uniformity of the loaded into the micropores of silica support $MnFe_2O_4$ species, as was also seen from the nitrogen physisorption, XRD and Moessbauer data. The TPR-TG profile of MnFe/ACP demonstrates not only easier reduction decomposition of loaded $MnFe_2O_4$ phase, but also some significant changes with the AC above 700 K, most probably promoted by the formation of metallic Fe^0. Contrary to other KIT-6 loaded ferrites, TPR-DTG profile of ZnFe/KIT-6 consists

of two overlapping effects, which in consistent with the XRD and Moessbauer measurements, could be due to the reduction of a mixture of Fe_2O_3 and $ZnFe_2O_4$. The reduction transformation of $ZnFe_2O_4$ seems to be facilitated on the ACP support and similarly to MnFe/ACP and CuFe/ACP, here significant changes with ACP occur above 700 K.

Catalytic tests

In Fig. 5a is presented the evolution of methanol decomposition on various modifications with the temperature increase. All materials exhibit catalytic activity above 600 K and CO, CH_4 and CO_2 in different proportion (Fig. 5b) are the only detected carbon-containing products. Among the KIT-6 based materials, the best catalytic activity with relatively high selectivity to CO and CH_4 is detected for CuFe/KIT-6. According to the XRD, Moessbauer and nitrogen physisorption measurements (Fig. 1, Tables 1 and 2) this could be assigned to the formation of finely dispersed $CuFe_2O_4$ particles, almost randomly distributed in the micro-mesopores of the sicila matrix. The latter stabilizes them also against phase transformations under the reaction medium as was illustrated by the Moessbauer analyses (Fig. 3b, Table 2). We could speculate that the preferable location of copper ions on the most exposed to the reactants octahedral positions in the inverse $CuFe_2O_4$ spinel structure provokes the activity of Cu^{2+}-Cu^{1+} redox pairs, which ensure high catalytic activity at relatively low temperature. However the Cu-Fe modification does not exhibit high catalytic activity when ACP is used as a host matrix. In accordance with the physicochemical measurements, this could be due to the limited formation of $CuFe_2O_4$ on the support with high reduction ability, like ACP. Here, during the catalyst preparation procedure, segregation of relatively large and low active Cu^0 and defective $Cu_xFe_{3-x}O_4$ nanoparticles, which also change under the reaction medium to Fe_3C (Fig. 3b, Table 2), is observed. Obviously, the predominant location of Zn^{2+} ions on tetrahedral positions of normal $ZnFe_2O_4$ spinel provides the activity of Fe^{3+}-Fe^{2+} redox pairs, situated on the octahedral position. The predominant location of metal oxide species into the mesopores of ACP seems to facilitate their intimate contact leading to the formation of finely dispersed $ZnFe_2O_4$ (Figs.1 and 3a, Tables 1 and 2). More over, the significantly low reduction ability of this ferrite phase (Fig. 4) ensures its preservation against decomposition under the reduction reaction medium even in the presence of carbon support and this is well illustrated by the Moessbauer spectra after the catalytic test (Fig. 3b, Table 2). This provides extremely high catalytic activity for ZnFe/ACP (Fig. 5). In accordance with the nitrogen physisorption, Moessbauer and XRD measurements (Tables 1 and 2 and Figs. 1 and 3a), it could be concluded that the blocking of active phase in the micropores of KIT-6 support renders difficult the formation of $ZnFe_2O_4$ phase and provokes segregation of less active individual Fe_2O_3. In case of mixed $MnFe_2O_4$ spinel ferrite (Fig. 5), the partial substitution of Mn^{2+} ions in tetrahedral position forces the migration of Fe^{2+} ions in octahedral one, which ensures the activity of Fe^{2+}-Fe^{3+} redox pairs.

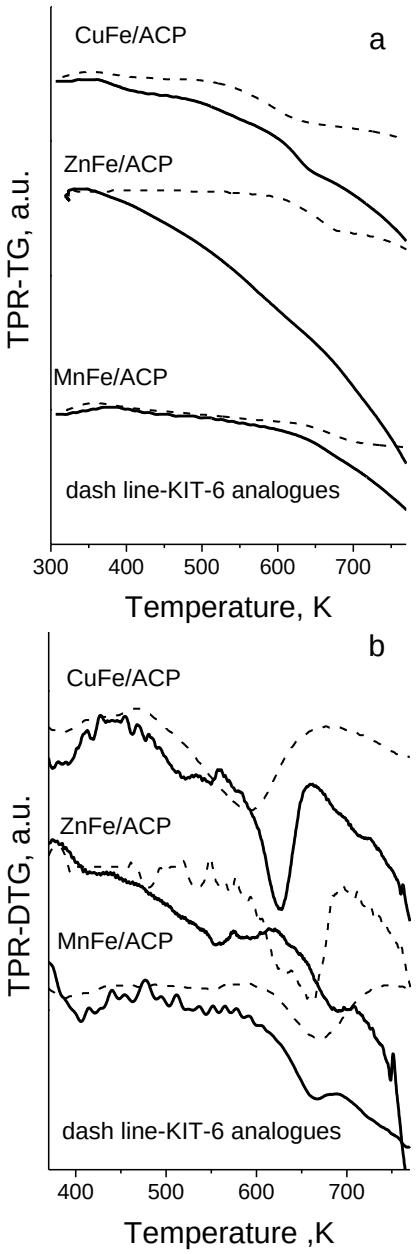

Fig. 4. TPR-TG (a) and TPR-DTG (b) data for ACP and KIT-6 modifications.

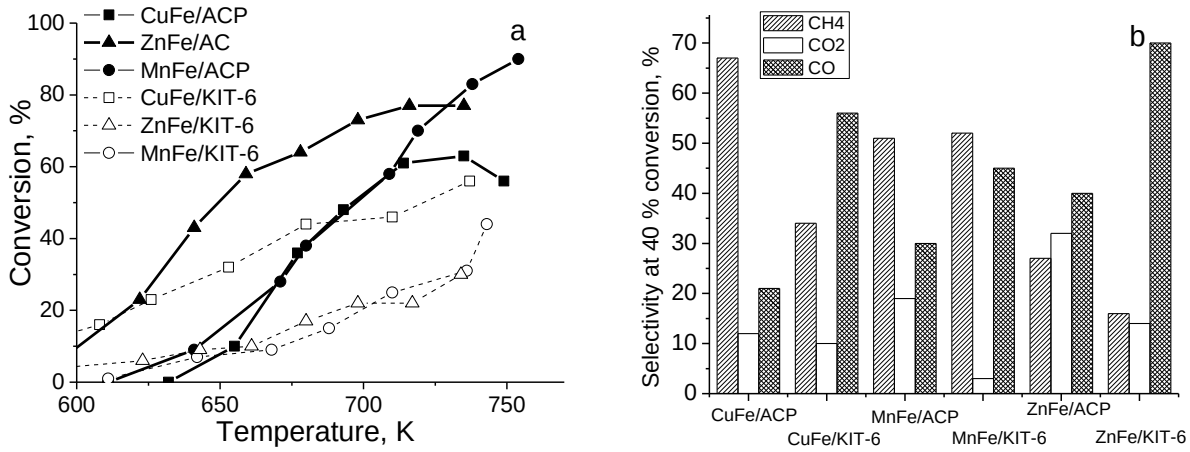

Fig. 5. Temperature dependency of methanol conversion (a) and products distribution at 40% conversion (b) for various samples.

On contrary to $ZnFe_2O_4$, we expect that the substitution with larger Mn^{2+} ions expands the spinel lattice, which suppresses the electron exchange in the Fe^{2+}-Fe^{3+} redox pairs and leads to lower catalytic activity and some differences in the selectivity. The significantly lower catalytic activity of $MnFe_2O_4$ species, hosted in the KIT-6 as compared to ACP is probably provoked by their lower accessibility for the reactant molecules due to the predominant location in the micropores of silica matrix (Table 1).

CONCLUSION

Activated carbon obtained from agriculture residues (peach stones) could be suitable host matrix for the stabilization of finely dispersed ferrite nanoparticles. Their formation is strongly controlled by the texture characteristics and the reduction properties of carbon support. $ZnFe_2O_4$ is appropriate ferrite phase for the preparation of highly active catalysts for methanol decomposition.

Acknowledgements: *Financial support Bulgarian Scientific Fund, project FNI E02/2/2014, is acknowledged.*

REFERENCES

1. A. Pohar, D. Belavi, G. Dolan, S. Hocevar, *J. Power Sources*, **256**, 80 (2014).
2. S. T. Yong, C. W. Ooi, S. P. Chai, X. S. Wu, *Int. J. Hydrogen Energy*, **38**, 9541 (2013).
3. A. Evdou, V. Zaspalis, L. Nalbandian, *Fuel*, **165**, 367 (2016).
4. M. Santiago, K. Barbera, C. Ferreira, D. Curulla-Ferré, P. Kolb, J. Pérez-Ramírez, *Catal. Commun*., **21**, 63 (2012).
5. M. Pori, B. Likozar, M.Marinšek, Z. C. Orel, *Fuel Proc. Technol*., **146**, 39 (2016).
6. E. Manova, T. Tsoncheva, D. Paneva, J. L. Rehspringer, K. Tenchev, I. Mitov, L. Petrov, *Appl. Catal. A: General*, **317**, 34 (2007).
7. T. Tsoncheva, E. Manova, N.Velinov, D. Paneva, M. Popova, B. Kunev, K. Tenchev, I. Mitov, *Catal. Commun*., **12**, 105 (2010).
8. E. Manova , T. Tsoncheva, D. Paneva, M. Popova , N. Velinov, B. Kunev, K. Tenchev, I. Mitov, *J. Solid State Chem*., **184**, 1153 (2011).
9. N. Velinov, E. Manova, T. Tsoncheva, C. Estournès, D. Paneva, K. Tenchev, V. Perkova, K. Koleva, B. Kunev, I. Mitov, *Solid State Sci*., **14**, 1092 (2012).
10. N. Velinov, K. Koleva, T.Tsoncheva, E. Manova, D. Paneva, K. Tenchev, B. Kunev, I. Mitov, *Catal. Commun*., **32**, 41 (2013).
11. H. Xue, Z. Li, X. Wang, X. Fu, *Mater. Lett*., **61**, 347 (2007).
12. D. H. K. Reddy, Y.-S. Yun, *Coord. Chem. Rev*., **315**, 90 (2016).
13. M. S. Podder, C. B. Majumder, *Ground water Sust. Devel*., **2-3**, 53 (2016).
14. K.-W. Jung, B. Hyun Choi, M.-J. Hwang, T.-U. Jeong, K.-H. Ahn, *Biores. Technol*., **219**, 185 (2016).
15. T. Tsoncheva, I. Genova, D. Paneva, M. Dimitrov, B. Tsyntsarski, N. Velinov, R. Ivanova, G. Issa, D. Kovacheva, T. Budinova, I. Mitov, N. Petrov, *Solid State Sci*., **48**, 286 (2015).
16. B. Tsyntsarski, I. Stoycheva, T. Tsoncheva, I. Genova, M. Dimitrov, B. Petrova, D. Paneva, Z. Cherkezova-Zheleva, T. Budinova, H. Kolev, A. Gomis-Berenguer, C. O. Ania, I. Mitov, N. Petrov, *Fuel Process.Technol.*, **137**, 139 (2015).

17. T. Tsoncheva, A. Mileva, D. Paneva, D. Kovacheva, I. Spassova, D. Nihtianova, P. Markov, N. Petrov, I. Mitov, *Micropor. Mesopor. Mater*., **229**, 59 (2016).
18. T. Tsoncheva, I. Genova, M. Stoyanova, M. Pohl, R. Nickolov, M. Dimitrov, E. Priboczki, M. Mihaylov, D. Kovacheva, K. Hadjiivanov, *Appl.Catal.B: Env*., **147**, 684 (2014).
19. H. P. Boehm, Chemical Identification of Surface Groups, *Adv. Catal. Related Subjects,* **16,** 179 (1966).
20. T. H. Liou, S. J. Wu, *J. Hazard. Mater.*, **171**, 693, (2009).
21. F. Rodriguez-Reinoso, *Carbon*, **36**, 159 (1998).
22. S. Briceño, W. Escamilla, P. Silva, J. García, H. Del Castillo, M. Villarroel, J. P. Rodriguez, M. A. Ramos, R. Morales, Y. Diaz, *J. Magnet.Magnet. Mater*., **360**, 67 (2014).
23. M. Florea, M. Alifanti, V. I. Parvulescu, D. Mihaila-Tarabasanu, L. Diamandescu, M. Feder, C. Negrila, L. Frunza, *Catal. Today*, **141**, 361 (2009).
24. X. Li, Y. Hou, Q. Zhao, L. Wang, *J. Coll. Int. Sci*., **358**, 102 (2011).
25. R. Olar, M. Badea, L. Diamandescu, E. Cristurean, D. Marinescu, D. Mihaila-Tarabasanu, N. Stanica, M. Brezeanu, *J. Alloys Comp*., **363**, 262 (2004).
26. J. A. Zawicki, H. A. Allsop, *J. Nuclear. Mater*., **240**, 22 (1996).
27. N. Thouchprasitchai, A. Luengnaruemitchai, S. Pongstabodee, J. *Ind. Eng. Chem*., **19**, 1483 (2013).
28. Z. H. Chonco, L. Lodya, M. Claeys, E. van Steen, *J. Catal*., **308**, 363 (2013).

КАТАЛИЗАТОРИ ЗА ОСВОБОЖДАВАНЕ НА ВОДОРОД ОТ МЕТАНОЛ НА ОСНОВАТА НА МЕДЕН, ЦИНКОВ И МАНГАНОВ ШПИНЕЛНИ ФЕРИТИ, НАНЕСЕНИ ВЪРХУ АКТИВЕН ВЪГЛЕН ОТ ОТПАДНА БИОМАСА

Т. С. Цончева[1]*, Г. С. Исса[1], А. Б. Милева[1], Р. Н. Иванова[1], М. Д. Димитров[1], И. П. Спасова[2], Д. Г. Ковачева[2], Д. Г. Панева[3], Н. И. Велинов[3], Б. Г. Цинцарски[1], Н. В. Петров[1]

[1] Институт по органична химия с Център по фитохимия, Българска академия на науките, 1113 София, България
[2] Институт по обща и неорганична химия, Българска академия на науките, 1113 София, България
[3] Институт по катализ, Българска академия на науките, 1113 София, България

Постъпила на 13 февруари 2017 г.; Коригирана на 06 март 2017 г.

(Резюме)

Активен въглен, получен от костилки от праскови, е използван като носител на наноразмерни MFe_2O_4 (M = Cu, Zn, Mn) шпинелни ферити. Получените композити са характеризирани с физисорбция на азот, рентгеноструктурен анализ, УВ, ФТИР и Мьосбауерова спектроскопии и ТПР с водород. Каталитичното поведение на образците е изследвано в разлагане на метанол, с оглед потенциалното му приложение като носител на водород. Катализаторите, получени на основата на активен въглен, показват по-висока активност, но по-ниска селективност до синтез газ, в сравнение с аналозите им, получени при използването на мезопорест силикат. $ZnFe_2O_4$ е най-подходяща активна фаза върху активен въглен, докато $CuFe_2O_4$ показва най-висока активност върху силикатен носител. Дискутирана е подробно ролята на различните носители върху формирането на каталитично активната фаза.